Science Advances
AAAS

advances.sciencemag.org/cgi/content/full/5/2/eaav5749/DC1

Supplementary Materials for

Fully rubbery integrated electronics from high effective mobility intrinsically stretchable semiconductors

Kyoseung Sim, Zhoulyu Rao, Hae-Jin Kim, Anish Thukral, Hyunseok Shim, Cunjiang Yu*

*Corresponding author. Email: cy15@uh.edu

Published 1 February 2019, *Sci. Adv.* **5**, eaav5749 (2019)
DOI: 10.1126/sciadv.aav5749

This PDF file includes:

Section S1. Analysis of enhanced effective mobility in m-CNT–doped P3HT-NFs/PDMS
Section S2. Contact resistance analysis through the TLM
Section S3. Calculation of mobility and threshold voltage
Section S4. Circuit architecture designs of the rubbery inverters NAND and NOR
Section S5. Cross-talk evaluation of the pressure-sensitive rubber
Section S6. Data acquisition of active matrix rubbery tactile sensing skin
Fig. S1. Preparation of AgNPs-AuNWs/PDMS through a galvanic replacement process.
Fig. S2. SEM image of ion gel.
Fig. S3. Areal fraction of m-CNT on the semiconducting layer after dry transfer.
Fig. S4. Output characteristics of the devices with different m-CNT concentrations.
Fig. S5. Transfer characteristics of the devices with P3HT/m-CNT and P3HT-NFs/PDMS/m-CNT.
Fig. S6. Summary list of a few different semiconducting material–based transistors.
Fig. S7. Effective μ_{FE} enhancement mechanism in m-CNT–doped P3HT-NFs/PDMS.
Fig. S8. m-CNT source and drain electrode–based transistor.
Fig. S9. Schematic fabrication process of rubbery transistor array.
Fig. S10. Hysteresis loop of the transfer curve for the rubbery transistor at a scan rate of 10 mV/s.
Fig. S11. I_{on}/I_{off} map of all 64 rubbery transistors for an 8 by 8 array.
Fig. S12. Hysteresis loop of the VTC curve for the rubbery inverter at a scan rate of 10 mV/s.
Fig. S13. Truth tables for rubbery NAND and NOR gates.
Fig. S14. Static output characteristics of the rubbery NAND and NOR gates.
Fig. S15. Physical integration of the fully rubbery tactile sensing skin.
Fig. S16. Schematic fabrication processes of the rubbery tactile sensing skin with 8 by 8 transistor array based on an active matrix readout.
Fig. S17. Resistance change of the pressure-sensitive rubber sheet depending on applied pressure.
Fig. S18. Electrical measurement of the pressure-sensitive rubber sheet.

Fig. S19. Circuit diagram of the 8 by 8 active matrix–based rubbery tactile sensing skin.
Fig. S20. Output voltage measurement of the rubbery tactile sensing skin.
Reference (*44*)

Section S1. Analysis of enhanced effective mobility in m-CNT–doped P3HT-NFs/PDMS

The comparison of transconductance (g_m) between the materials with and without m-CNTs provides a systematic explanation of the enhancement of effective field effect mobility (μ_{FE}), as illustrated in fig. S7. The similar effective moblity enhancement has been realized in other rigid semiconductor composite (*24*). In a transistor, the g_m can be obtained by

$$g_m = \frac{\delta I_{DS}}{\delta V_{GS}} = \frac{\Delta \frac{V_{DS}}{R_{CH}}}{V_{GS} - V_{TH}} \approx \frac{\frac{V_{DS}}{R_{ON}} - \frac{V_{DS}}{R_{OFF}}}{V_{GS} - V_{TH}} \tag{S1}$$

where I_{DS} is the current, V_{GS} is the source-gate voltage, V_{TH} is the threshold voltage, V_{DS} is the source-drain voltage, R_{CH} is the channel resistance, R_{ON} is the resistance when the device is on, and R_{OFF} is the resistance when the device is turned off.

One considers the P3HT-NFs/PDMS rubbery transistors as n parts individual small transistors connected in series. Each small transistor has a resistance R_i at the ON state and the $R_{OFF} >> R_{ON}$, therefore, for P3HT-NFs/PDMS without m-CNT doping, the transconductance ($g_{P3HT\text{-}NFs}$) is

$$g_{P3HT-NFs} \approx \frac{\frac{V_{DS}}{R_{ON}} - \frac{V_{DS}}{R_{OFF}}}{V_{GS} - V_{TH}} \approx \frac{V_{DS}}{V_{GS} - V_{TH}} \frac{1}{nR_i} \tag{S2}$$

For the m-CNT doped semiconductor, there are occasions when the m-CNT shortens the individual small P3HT-NFs transistors. Here, the resistance of an individual m-CNT can be ignored. Assuming that m (m < n) parts of the individual small P3HT-NFs transistors are shortened by the m-CNT, the transconductance of the doped semiconductor ($g_{m\text{-}CNT/P3HT\text{-}NFs}$) is

$$g_{m-CNT/P3HT-NFs} \approx \frac{V_{DS}}{V_{GS} - V_{TH}} \frac{1}{(n-m)R_i} \tag{S3}$$

Therefore, the μ_{FE} of transistor based on the m-CNT doped P3HT-NFs/PDMS ($\mu_{m\text{-}CNT/P3HT\text{-}NFs}$) is higher than that based on the P3HT-NFs/PDMS ($\mu_{P3HT\text{-}NFs}$)

$$\mu_{m-CNT/P3HT-NFs} / \mu_{P3HT-NFs} = g_{m-CNT/P3HT-NFs} / g_{P3HT-NFs} = \frac{n}{n-m} \tag{S4}$$

$$\mu_{m-CNT/P3HT-NFs} \approx \frac{n}{(n-m)} \mu_{P3HT-NFs} \tag{S5}$$

The above information qualitatively explains the μ_{FE} enhancement in this intrinsically stretchable semiconductor based transistor.

Section S2. Contact resistance analysis through the TLM

The contact resistance (R_C) between m-CNT and P3HT-NFs was extracted through the transfer length method (TLM). The ON resistance of the transistor (R_{ON}) can be expressed by (*29, 44*)

$$R_{ON}(L) = R_{CH}(L) + R_C \tag{S6}$$

where R_{CH} is the channel-length (L)-dependent channel resistance. The R_{ON} with a different channel length was characterized as V_{GS} of -3V and V_{DS} of -0.2 V ($V_{DS} << V_{GS} - V_{TH}$). Since the R_C is constant regardless of the channel length, the width-normalized R_C ($R_C \cdot W$) can be extracted from the y-intercept of the extrapolated plot of the width-normalized R_{ON} ($R_{ON} \cdot W$) versus L. The fitted plot in Fig. 4 shows a slope of 3.912 ± 0.34, a y-intercept of 271.59 ± 65.39 and an R^2 of 0.90.

Section S3. Calculation of mobility and threshold voltage

The μ_{FE} was calculated by fitting the plot of the linear regime in the curve of $\sqrt{I_{DS}}$ versus V_{GS} based on the following equation

$$I_{DS} = \frac{WC_i \mu_{FE}}{2L}(V_{GS} - V_{TH})^2 \tag{S7}$$

$$\sqrt{I_{DS}} = \sqrt{\frac{WC_i \mu_{FE}}{2L}}(V_{GS} - V_{TH}) = \sqrt{\frac{WC_i \mu_{FE}}{2L}}V_{GS} - \sqrt{\frac{WC_i \mu_{FE}}{2L}}V_{TH} \tag{S8}$$

$$Slope = \sqrt{\frac{WC_i \mu_{FE}}{2L}} \tag{S9}$$

$$\mu_{FE} = \frac{2L}{WC_i}(Slope)^2 \tag{S10}$$

where L, W, and C_i are the channel length, the width, and the specific capacitance of the gate dielectrics, respectively. The threshold voltage (V_{TH}) is defined by the x-intercept of the extrapolation of the fitted curve.

Section S4. Circuit architecture designs of the rubbery inverters NAND and NOR

The rubbery inverter was structured as a Zero-V_{GS} load device with two p-type stretchable transistors for the unipolar transistor logic gate. Both the driver and the load transistors were integrated serially. Specifically, the rubbery inverter consisted of two rubbery transistors with a channel width ratio of 1:4 (Driver transistor : Load transistor) and the same channel length.

Both the rubbery NAND and NOR gates were constructed based on two drivers ($T_{D,A}$ and $T_{D,B}$) and one load (T_L) rubbery transistor. The two rubbery driver transistors were connected in parallel for NAND and serially for NOR, and then serially connected to load transistors. The channel length of all the drivers and load transistors were the same; the ratios of the channel

width of the driver to the load of the rubbery transistors were 1 to 4 for the NAND and 1 to 3 for the NOR logic gates.

Section S5. Cross-talk evaluation of the pressure-sensitive rubber

To evaluate the cross-talk of the pressure-sensitive rubber, two adjacent sensing pixels with metal-pressure sensitive rubber-metal structure were prepared through one common top electrode and two bottom electrodes for each pixel (#1 and #2 in fig. S16C). The electrodes employed Al tapes. A voltage of 0.01 V was applied between the common top electrode and the bottom electrode for #1; the current between them was measured during pressing and releasing. While the measured current sharply increased due to the decreased resistance of the pixel (#1) once it was pressed, no current change was observed when the other pixel (#2) was pressed. These results indicate that no current flows between adjacent sensing pixels through pressure-sensitive rubber, and therefore no cross-talk exists.

Section S6. Data acquisition of active matrix rubbery tactile sensing skin

Tactile sensing skin contact sites readout and mapping based on the 8 × 8 active matrix were achieved by a data acquisition system. The schematic circuit diagram of the active matrix and interface with the data acquisition are shown in fig. S17. To apply voltage in 8-word lines and V_{DD}, the devices were interfaced to the NI PXI-6723 (National Instruments) through a SCB-68 shielded I/O connector block. An NI PXI-6363 (National Instruments) was interfaced through another SCB-68 shielded I/O connector block for voltage readout from the bit line of the active matrix rubbery tactile sensing skin.

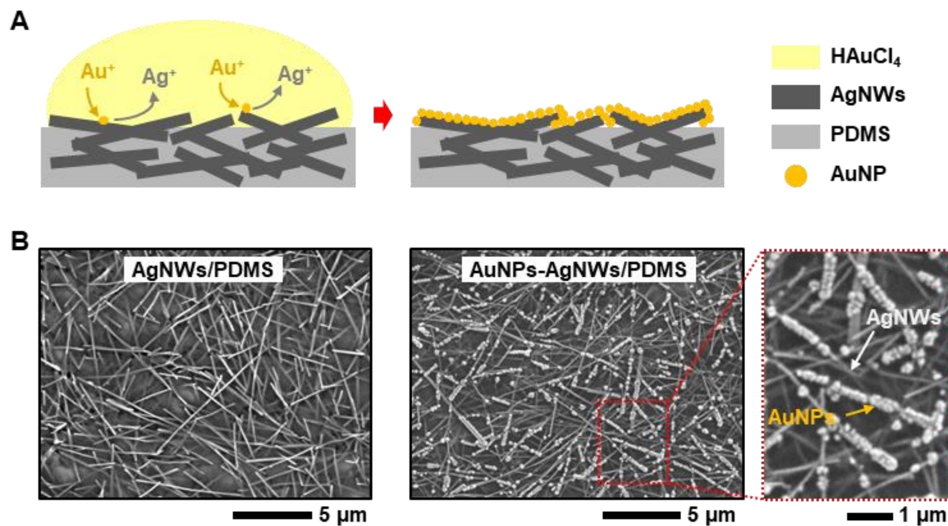

Fig. S1. Preparation of AgNPs-AuNWs/PDMS through a galvanic replacement process. (**A**) Schematic illustration of the galvanic replacement process. (**B**) Scanning electron microscope (SEM) images of the AgNWs/PDMS (left) and the AuNPs-AgNWs/PDMS (right) electrodes.

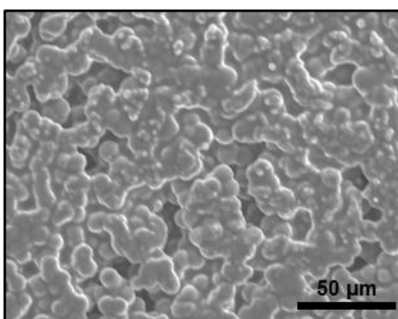

Fig. S2. SEM image of ion gel.

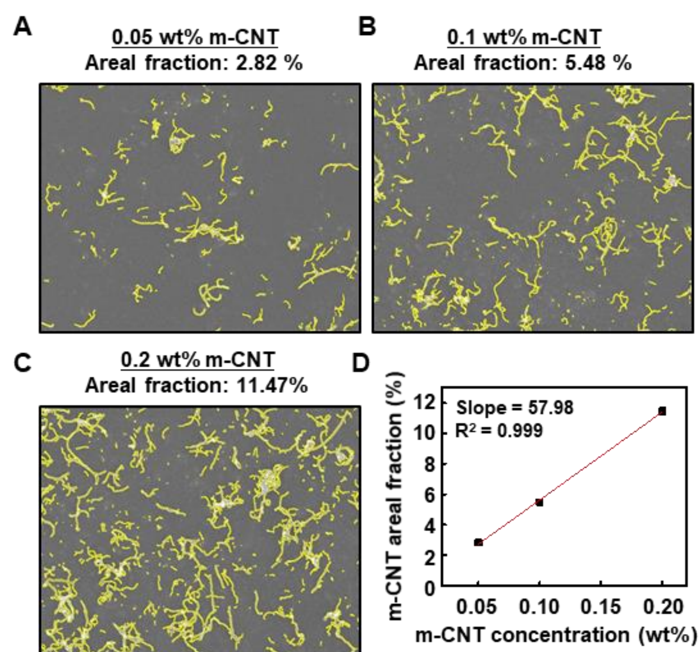

Fig. S3. Areal fraction of m-CNT on the semiconducting layer after dry transfer. (**A** to **C**) The area selection with the m-CNTs highlighted in yellow for calculating the $f_{area,m\text{-}CNT}$. (**D**), Linear relationship between the $f_{area,m\text{-}CNT}$ and the m-CNT concentration of the suspension

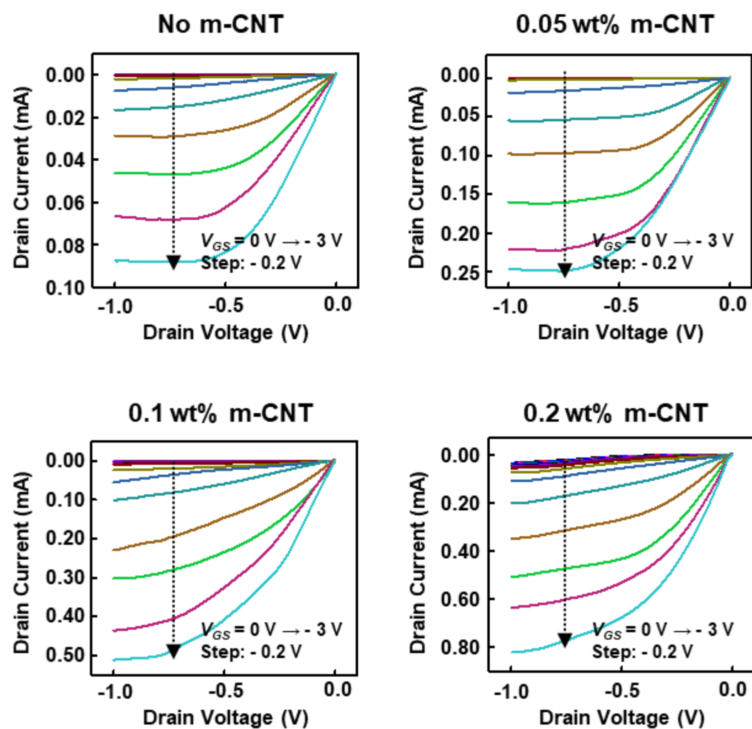

Fig. S4. Output characteristics of the devices with different m-CNT concentrations.

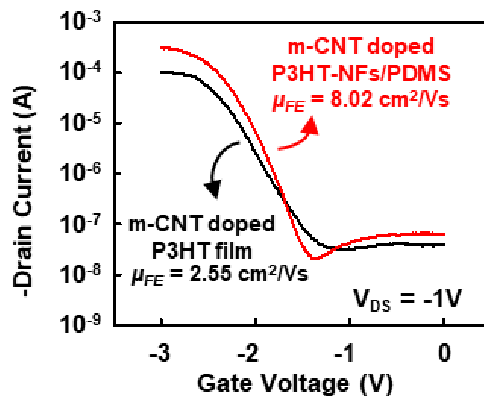

Fig. S5. Transfer characteristics of the devices with P3HT/m-CNT and P3HT-NFs/PDMS/m-CNT.

Semiconducting material	Stretchable (Yes/No)	Stretching direction	Mobility under 0% (cm²/Vs)	Mobility under 50% (cm²/Vs)	Note
m-CNT doped P3HT-NFs/PDMS	Yes	// channel length	7.46	3.57	This work
	Yes	⊥ channel length	7.37	2.44	
P3HT-NFs/PDMS	Yes	// channel length	1.43	0.79	Ref. #21
	Yes	⊥ channel length	1.43	0.40	
m-CNT-doped P3HT film	No	N/A	2.55	N/A	A non-stretchable semiconductor without P3HT-NFs.

Fig. S6. Summary list of a few different semiconducting material–based transistors.

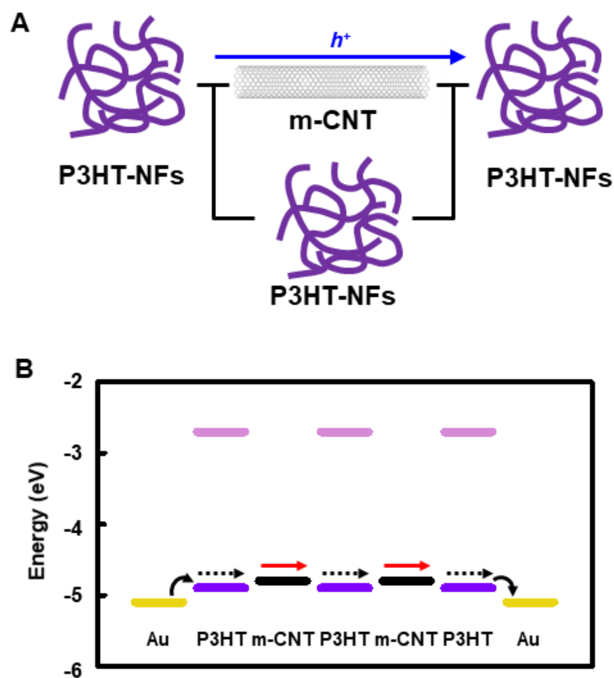

Fig. S7. Effective μ_{FE} enhancement mechanism in m-CNT–doped P3HT-NFs/PDMS. (**A**) Schematic illustration of the charge carrier transport routes. (**B**) The energy diagrams for Au, P3HT, and m-CNT.

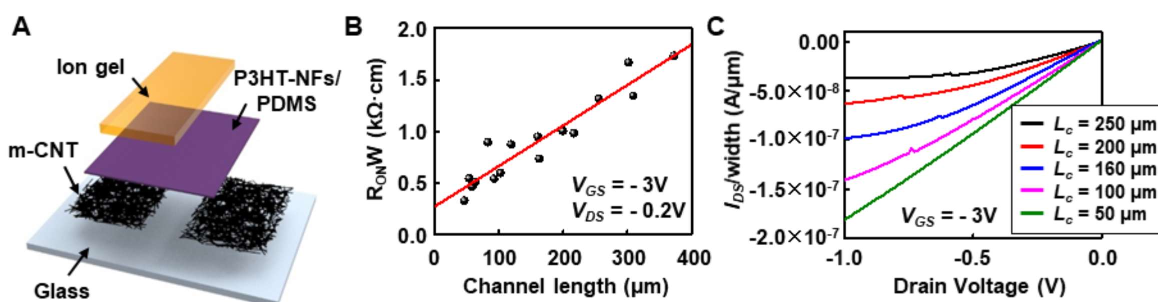

Fig. S8. m-CNT source and drain electrode–based transistor. (**A**) Schematic exploded view of P3HT-NFs/PDMS based device configuration using m-CNT as source and drain electrodes. (**B**) Plot of width normalized ON resistance ($R_{ON}W$) with different channel lengths. (**C**) Drain current at gate voltage of -3 V for transistors with various channel lengths.

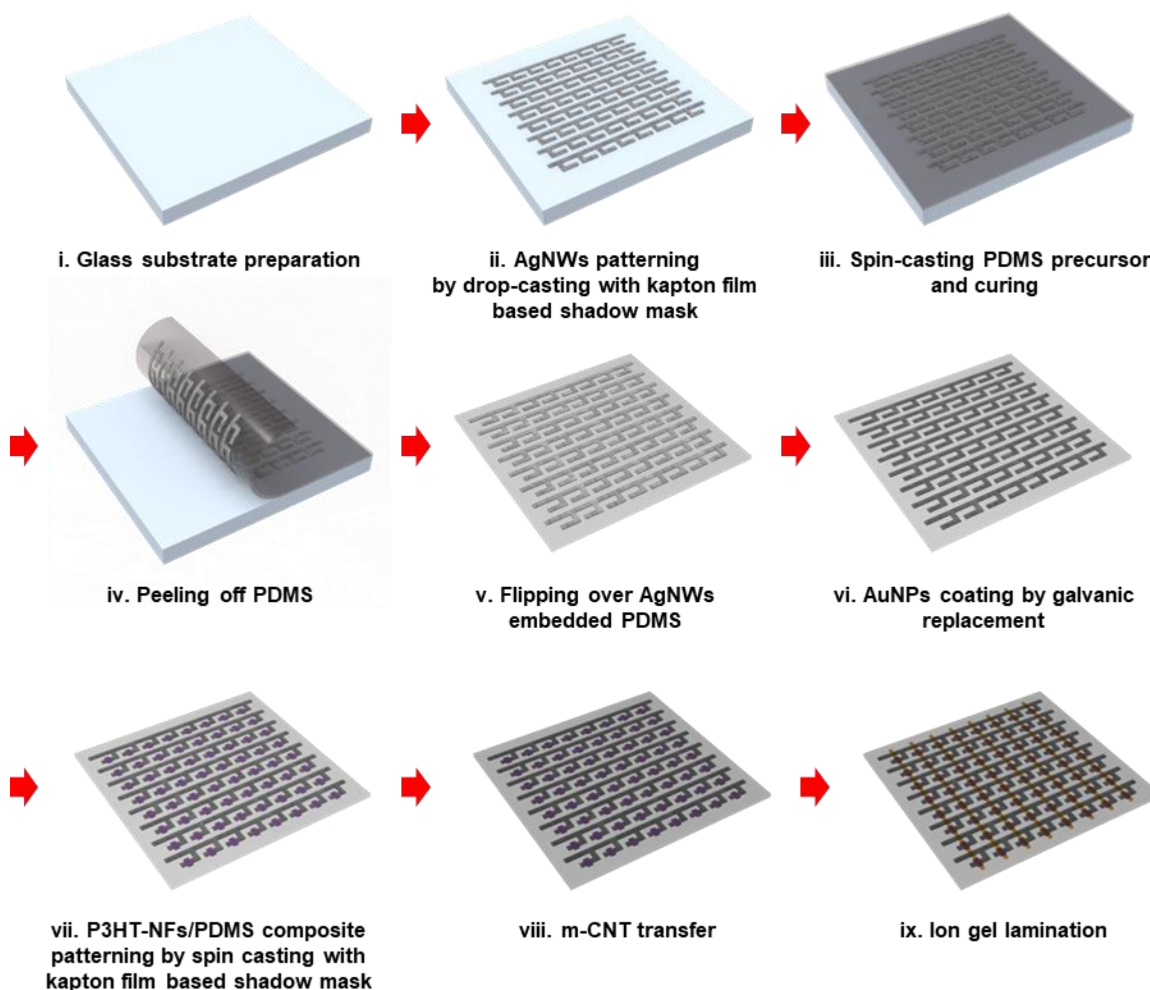

Fig. S9. Schematic fabrication process of rubbery transistor array.

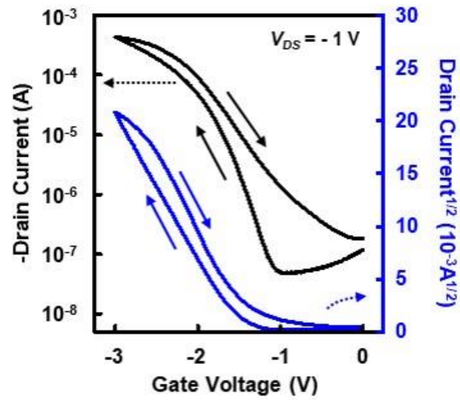

Fig. S10. Hysteresis loop of the transfer curve for the rubbery transistor at a scan rate of 10 mV/s.

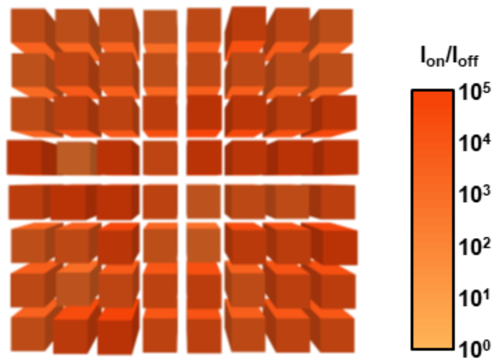

Fig. S11. I_{on}/I_{off} map of all 64 rubbery transistors for an 8 by 8 array.

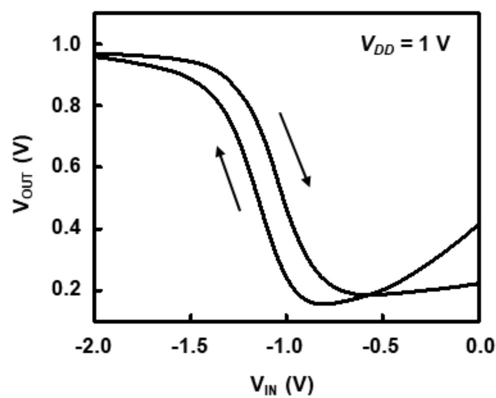

Fig. S12. Hysteresis loop of the VTC curve for the rubbery inverter at a scan rate of 10 mV/s.

Rubbery NAND gate

$V_{IN,A}$	$V_{IN,B}$	V_{OUT} (No strain)	V_{OUT} (50 % // L_C)	V_{OUT} (50 % ⊥ L_C)
0	0	1	1	1
1	0	1	1	1
0	1	1	1	1
1	1	0	0	0

Rubbery NOR gate

$V_{IN,A}$	$V_{IN,B}$	V_{OUT} (No strain)	V_{OUT} (50 % // L_C)	V_{OUT} (50 % ⊥ L_C)
0	0	1	1	1
1	0	0	0	0
0	1	0	0	0
1	1	0	0	0

Fig. S13. Truth tables for rubbery NAND and NOR gates.

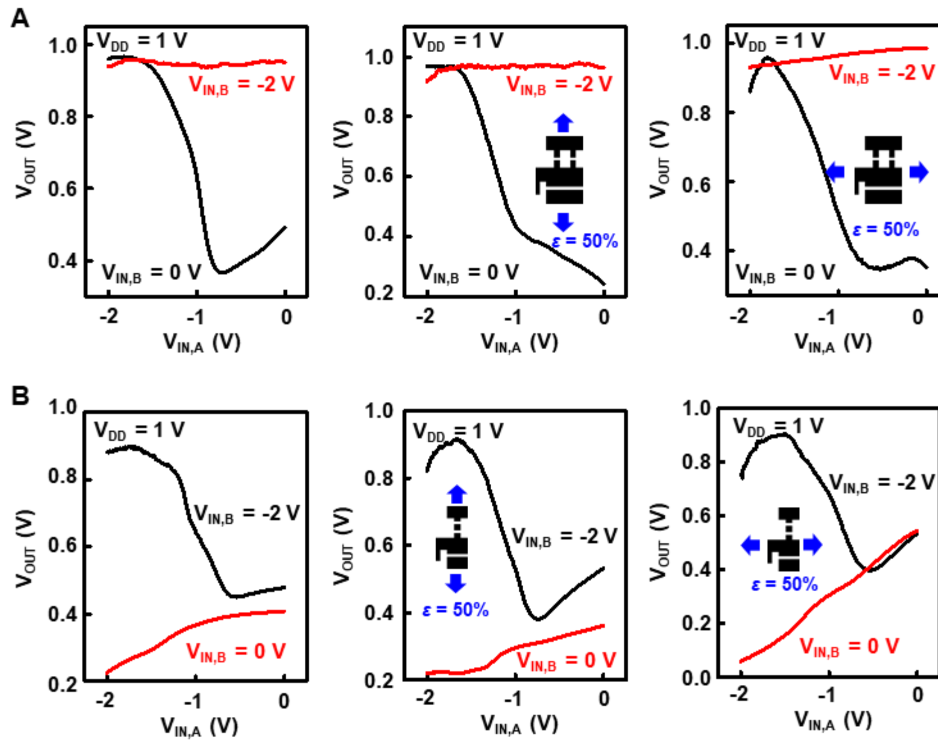

Fig. S14. Static output characteristics of the rubbery NAND and NOR gates. (**A**) Output voltage of NAND gate under mechanical strains of 0% (left) and 50% (middle) along and (right) perpendicular to the channel length direction. (**B**) Output voltage of NAND gate under mechanical strains of 0% (left) and 50% (middle) along and (right) perpendicular to the channel length direction.

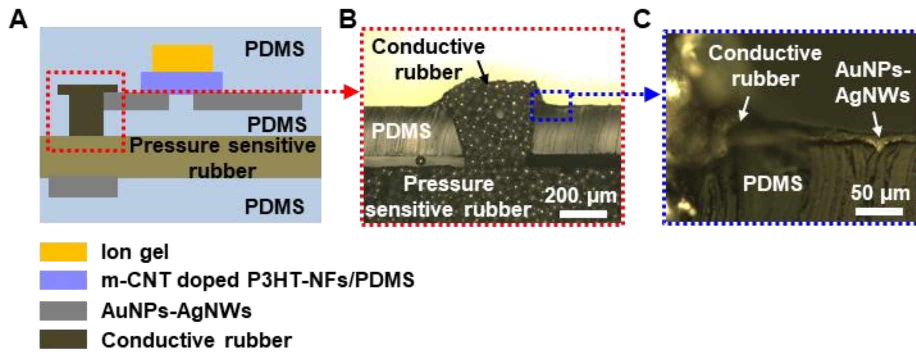

Fig. S15. Physical integration of the fully rubbery tactile sensing skin. (**A**) Schematic cross-sectional structure of the fully rubbery tactile sensing skin. (**B** and **C**) Optical images of the connection between the pressure-sensitive rubber and AuNPs-AgNWs/PDMS by conductive rubber paste.

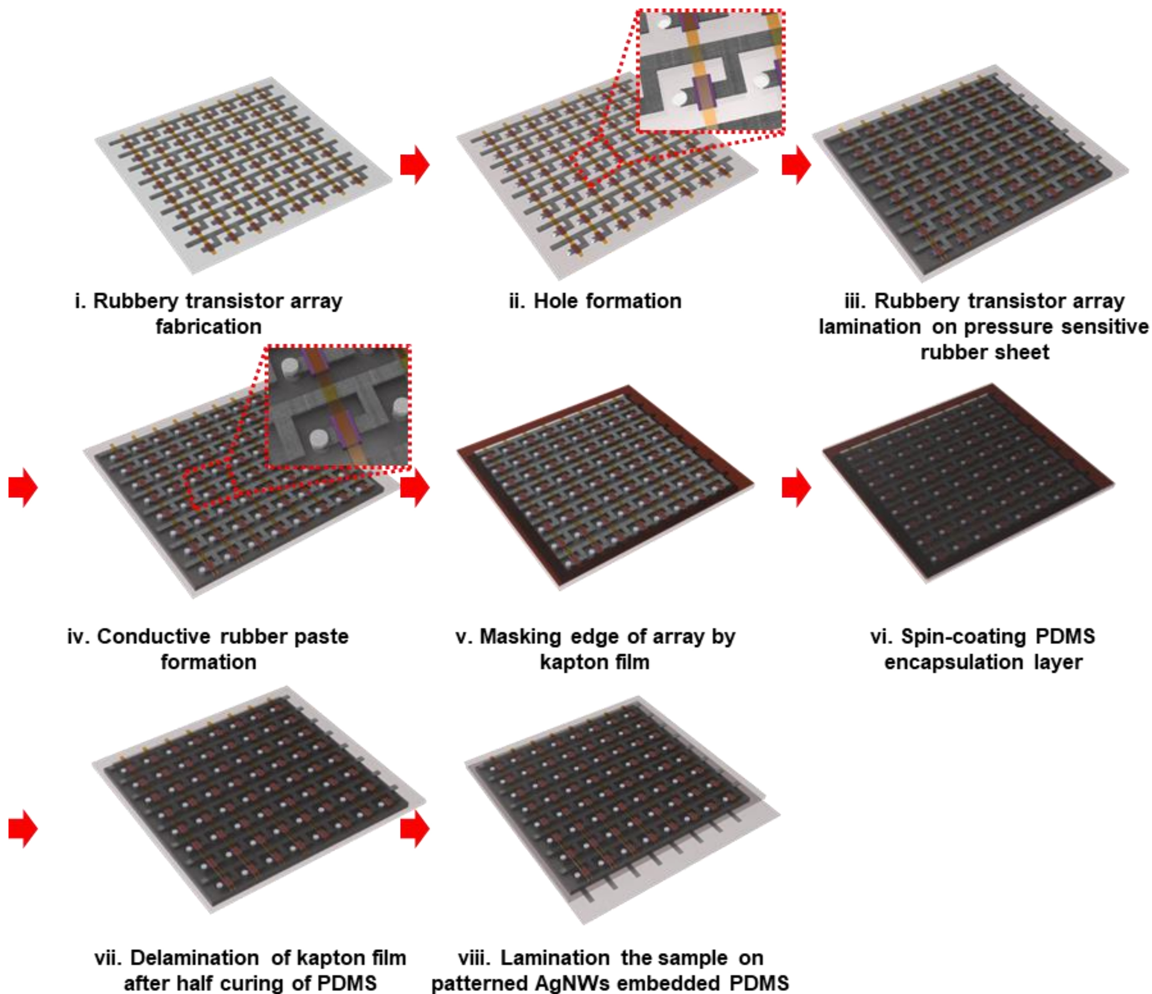

Fig. S16. Schematic fabrication processes of the rubbery tactile sensing skin with 8 by 8 transistor array based on an active matrix readout.

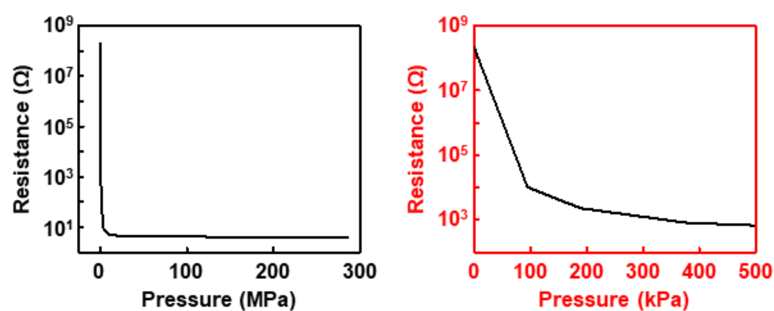

Fig. S17. Resistance change of the pressure-sensitive rubber sheet depending on applied pressure.

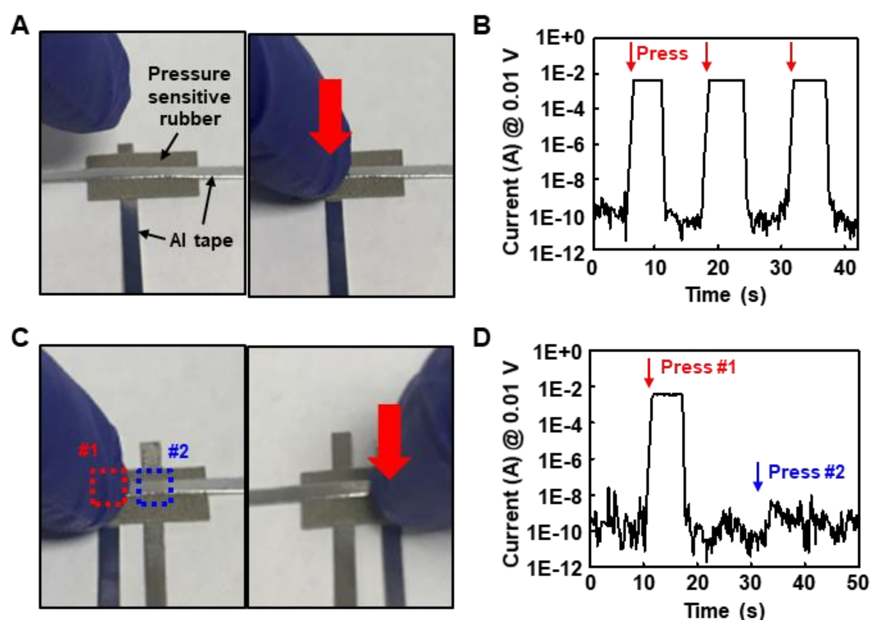

Fig. S18. Electrical measurement of the pressure-sensitive rubber sheet. (**A**) Optical images of pressure-sensitive rubber sheet testing. (**B**) Dynamic current response with and without pressing. (**C**) Optical images of the cross-talking test. (**D**) Dynamic current response of the cross-talking test.

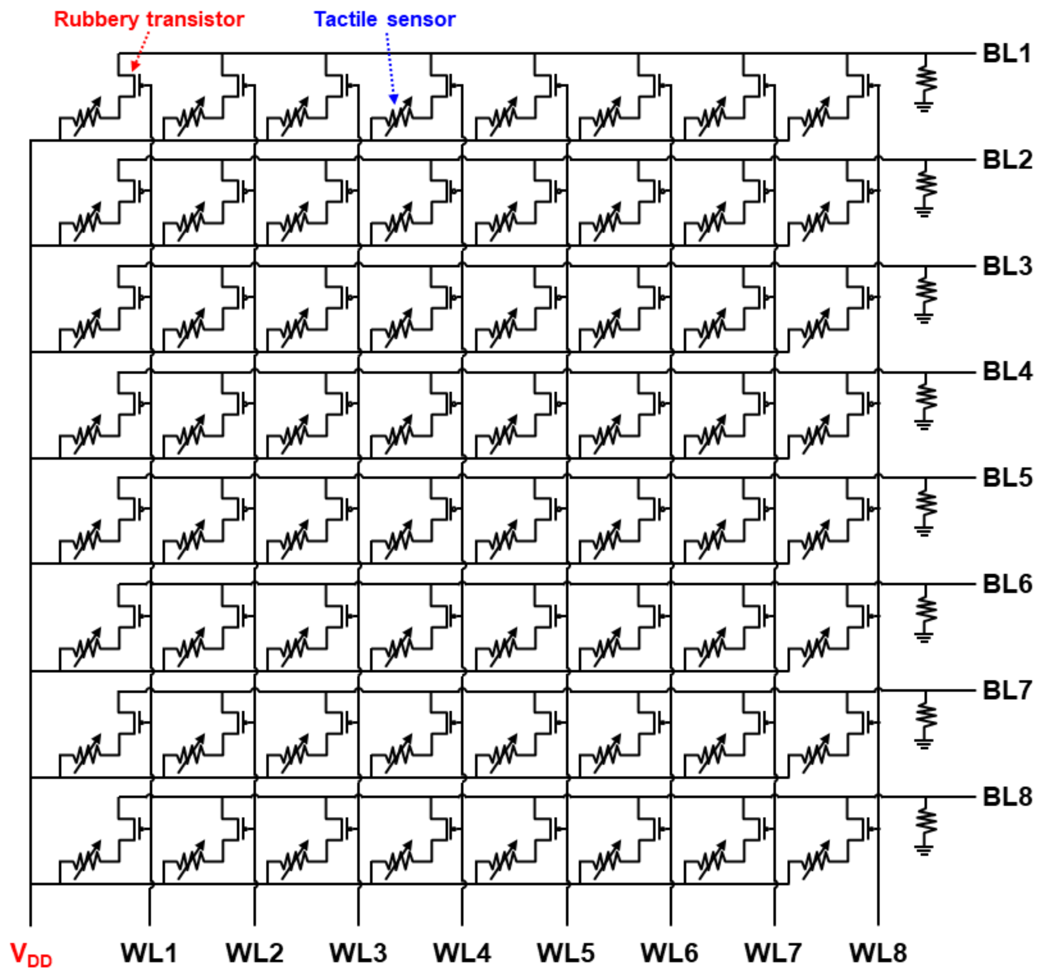

Fig. S19. Circuit diagram of the 8 by 8 active matrix–based rubbery tactile sensing skin.

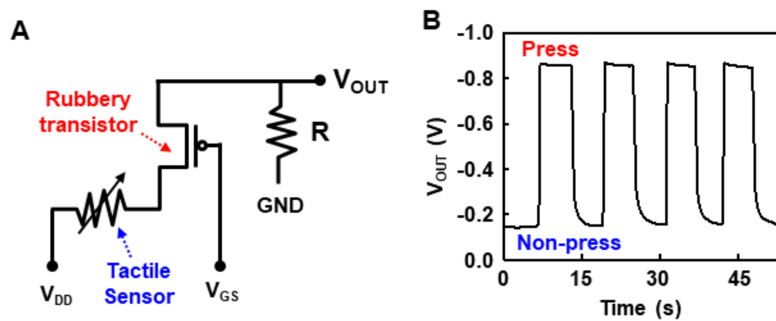

Fig. S20. Output voltage measurement of the rubbery tactile sensing skin. (**A**) Circuit diagram of an individual tactile sensing pixel for output voltage measurement. The shunt resistance (R) is 100 kΩ. (**B**) Dynamic output voltage change during cyclic pressing and releasing of a single pixel.